Nanoscale

PAPER

View Article Online
View Journal | View Issue

Cite this: *Nanoscale*, 2019, **11**, 10774

Ligand cleavage enables formation of 1,2-ethanedithiol capped colloidal quantum dot solids†

James Z. Fan, ‡[a] Andrew D. La Croix, ‡[b] Zhenyu Yang, [a] Emma Howard,[a] Rafael Quintero-Bermudez, [a] Larissa Levina,[a] Nicole M. Jenkinson, [b] Nathan J. Spear,[b,c] Yiying Li,[d] Olivier Ouellette, [a] Zheng-Hong Lu, [d] Edward H. Sargent [a] and Janet E. Macdonald *[b]

Received 28th March 2019,
Accepted 9th May 2019

DOI: 10.1039/c9nr02708d

rsc.li/nanoscale

Colloidal quantum dots have garnered significant interest in optoelectronics, particularly in quantum dot solar cells (QDSCs). Here we report QDSCs fabricated using a ligand that is modified, following film formation, such that it becomes an efficient hole transport layer. The ligand, *O*-((9*H*-fluoren-9-yl)methyl) *S*-(2-mercaptoethyl) carbonothioate (FMT), contains the surface ligand 1,2-ethanedithiol (EDT) protected at one end using fluorenylmethyloxycarbonyl (Fmoc). The strategy enables deprotection following colloidal deposition, producing films containing quantum dots whose surfaces are more thoroughly covered with the remaining EDT molecules. To compare fabrication methods, we deposited CQDs onto the active layer: in one case, the traditional EDT-PbS/EDT-PbS is used, while in the other EDT-PbS/FMT-PbS is used. The devices based on the new EDT/FMT match the PCE values of EDT/EDT controls, and maintain a higher PCE over an 18 day storage interval, a finding we attribute to an increased thiol coverage using the FMT protocol.

Solution-processed colloidal quantum dots (QDs) have attracted interest over the past decade in optoelectronic devices such as photovoltaics (PVs),[1] photodetectors,[2] lasers,[3] and light-emitting diodes.[4] Among the attractive properties of this type of material are the low cost of fabrication, the ability to tune the bandgap of the desired material for specific applications, and a high absorption per unit length.

Attention has been paid in recent studies to improving QD active layers in PV devices.[5] There has been less focus on the fabrication of the hole transport layer (HTL).[6–11] In earlier generations of CQD PV devices, HTLs typically consisted of MoO_x/Au/Ag anodes.[6,12,13] The MoO_x was sputtered onto the active layer, and Au and Ag were then sequentially thermally deposited. The MoO_x served as an Ohmic contact to the Au layer, facilitating hole transport, and protecting the CQD active layer from the noble metal evaporation process.[12] These devices reached power conversion efficiencies (PCE) of 9.5%.[13] In recent years, the choice of material has been switched to a solution processed layer such as QDs functionalized using a short chain thiol (*e.g.*, 1,2-ethanedithiol (EDT)).[14] EDT CQD films also provide an Ohmic contact with Au, and these HTL are processed in ambient conditions. The band position of halide-passivated PbS-active layers is deeper than that of EDT-PbS QDs, producing an HTL that accepts holes but blocks electrons.[14,15] Devices with EDT-PbS HTLs have recently exhibited PCEs that exceed 12%.[7,9,16–18]

Prior EDT-based HTLs have relied on a solid-state ligand exchange approach.[14] An oleic acid (OA)-capped PbS (OA-PbS) film is spin-coated onto a preformed PbS active layer, and ligand exchange within the new layer is achieved by soaking the film in an EDT solution. This process is generally repeated twice, and from henceforth the two film stack created will be referred to as EDT/EDT-PbS. This ligand exchange process, however, may disturb the QD surfaces because detachment of the $Pb(OA)_2$ species may occur and result in QDs with etched, fused, or oxidized surfaces.[19,20] Furthermore, unremoved Pb $(OA)_2$ impurities are a known source of trap states in PbS

[a]*Department of Electrical and Computer Engineering, University of Toronto, 10 King's College Road, Toronto, Ontario M5S 3G4, Canada. E-mail: ted.sargent@utoronto.ca*
[b]*Department of Chemistry, The Vanderbilt Institute of Nanoscale Science and Engineering, Vanderbilt University, Nashville, Tennessee 37235, USA. E-mail: janet.macdonald@vanderbilt.edu*
[c]*Vanderbilt Institute of Nanoscale Science and Engineering, Vanderbilt University, Nashville, Tennessee 37235, USA*
[d]*Department of Materials Science and Engineering, University of Toronto, 184 College Street, Toronto, ON M5S 3E4, Canada*
†Electronic supplementary information (ESI) available: Experimental methods and details, NMR, XPS, UPS, *J*–*V* sweeps. See DOI: 10.1039/c9nr02708d
‡These authors contributed equally to this work.

films.[21] Finally, unreacted free thiol groups (R-SH, R = alkyl or aryl chains) may form oxidation products from hydrolysis reactions in an ambient environment.[22,23] It has been previously shown that a moisture-free homogeneous ligand exchange can be performed by injecting alkanethiol capping ligands during the cooling stage directly after the synthesis of QDs in a one-pot reaction.[23–25] However, the direct injection of bifunctional EDT molecules during the synthesis stage causes crosslinking and aggregation of the PbS-QDs, resulting in a colloidally unstable solution.[10] The QDs must remain suspended post-synthesis in a homogenous suspension to allow the deposition of a uniform film. We sought therefore an alternative means to fabricate EDT HTL CQD films using a moisture-free homogenous ligand exchange process that enables post deposition modification to leave EDT on the PbS surface.

We pursued instead a strategy, intitiated by Turo *et al.*,[26] involving a cleavable functional group used within a stabilizing nanocrystal ligand. We synthesized *O*-((9*H*-fluoren-9-yl)methyl) *S*-(2-mercaptoethyl) carbonothioate (FMT), that contains both an ethanedithiol ligand and a fluorenylmethyloxycarbonyl (Fmoc) functional group (Fig. S1 and S2†). Fmoc is a protecting group which has been commonly used in solid state peptide synthesis where it is cleaved using a gentle organic base treatment.[27–29] We hypothesized that the FMT ligand would exchange with surface OA ligand, forming FMT-passivated PbS QDs. Molecular DFT calculations for FMT and EDT can be seen in Table S1† and indicate that the electron donating HOMO of the FMT is ~0.5 eV higher than that of EDT. This places the HOMO of FMT closer to that of the valence band of PbS (~−6.14 eV), allowing for a stronger bonding interaction.[30] These initially long bulky ligands stabilized the FMT-PbS QDs in a non-polar solvent, enabling the formation of uniform spin coated QD films. Following film deposition, the FMT was cleaved by a mild base to produce an EDT-PbS QD film as shown in Fig. 1.[27] We then applied this film preparation strategy to fabricate QD HTLs and studied the effect of

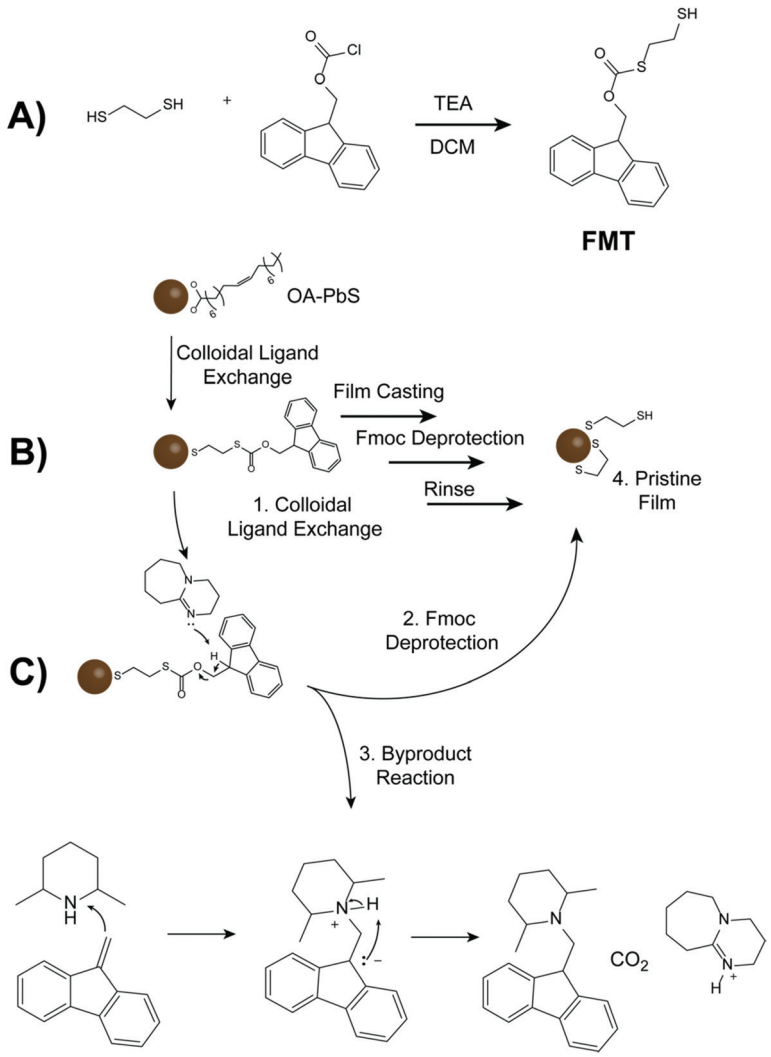

Fig. 1 (A) Synthesis of FMT. (B) Schematic illustration showing PbS thin film formation. Pristine oleic acid (OA)-capped PbS is exchanged in solution with FMT. After the facile cleavage with a base, byproducts are removed leaving behind only EDT. (C) Mechanism of Fmoc deprotection.

different bases upon the QD surfaces during the Fmoc deprotection. We will denote the cleaved FMT-PbS film as cFMT-PbS as the nomenclature for the rest of this manuscript. The EDT-capped PbS QD prepared by the traditional direct soak method will simply be denoted as EDT-PbS.

Experimental

Materials

Dichloromethane (DCM) (anhydrous, ≥99.8%), ethanedithiol (≥98.0%), trimethylamine (≥99.5%), ethyl acetate (EtOAc) (99.9%), hexanes (99.9%), $NaHCO_3$ (ACS grade), 1,8-diazabicyclo[5.4.0]undec-7-ene (DBU) (98%,), 2,6-lutidine (≥99%), 2,6-di-tert-butylpyridine (DTP) (≥97%), *cis*-2,6-dimethylpiperidine (DMPpy) (98%), and $MgSO_4$ (anhydrous, 97%) were purchased from Sigma-Aldrich. 9-Fluorenylmethyl chloroformate (Fmoc-Cl) (98%) was purchased from Oakwood Chemical. All materials were used as purchased without further purification.

Methods

FMT ligand synthesis

To a 100 ml round bottom flask with stir bar was added dry DCM, Fmoc-Cl (2.5 g, 10 mmol), and ethanedithiol (3.35 ml, 40 mmol). The reaction flask was sealed and maintained under inert atmosphere. Triethylamine (1.4 ml, 10 mmol) was added dropwise *via* syringe. The reaction was monitored *via* TLC (20% EtOAc/80% hexanes). Reactions typically completed within 15 min. The crude product was then washed 2 times with 5% $NaHCO_3$, followed by one brine wash. The organic layer was then dried over $MgSO_4$, solvent removed under reduced pressure. The resulting crude product was purified *via* column chromatography using a solvent gradient from 2.5% EtOAc/hexanes to 10% EtOAc/hexanes to yield a thick yellow oil. Yield: 1.74 g (55%) ^{1}H NMR (400 MHz, $CDCl_3$) δ 7.79 (d, 2H, J = 7.6 Hz), 7.60 (d, 2H, J = 7.1 Hz), 7.43 (t, 2H, J = 7.4 Hz), 7.34 (td, 2H, J = 7.5, 1.1 Hz), 4.52 (d, 2H, J = 7.4 Hz), 4.28 (t, 1H, J = 7.3 Hz), 3.08 (t, 2H, J = 6.7 Hz, 2.76 (m, 2H), 1.65 (t, 1H, J = 8.6 Hz). ^{13}C NMR (100 MHz, $CDCl_3$) δ 170.4 (C═O), 143.2, 141.3, 127.9, 127.2, 125.1, 120.1 (ArC), 69.2 (–CH–), 46.7(–CH2–), 35.0(–CH2–), 24.8(–CH2–) ppm.

OA-QD synthesis

The synthetic procedure for fabricating oleic acid capped PbS QDs are described in detail by Hines and Scholes.[31] Briefly, Pb-oleate is generated *in situ via* the dissolution of PbO in OA. At a temperature of 63 °C a mixture of trimethylsilyl sulfide in ODE was swiftly injected, and the reaction was allowed to cool to room temperature before purification *via* precipitation with acetone. A ^{1}H NMR of OA-PbS particles can be seen in Fig. S3† which shows the alkene protons from the oleic acid attached to the QD surface.

FMT-QD ligand exchange

To a solution of PbS QDs in $CHCl_3$ under vigorous stirring was added a solution of FMT in $CHCl_3$. After 30 min, the particles were precipitated with acetone three times, and the removal of the native OA ligands was verified *via* ^{1}H NMR spectroscopy by the loss of the vinylic proton signal (Fig. S4†).

To prepare FMT-PbS QDs for device fabrication, the FMT ligand (0.1 g, 0.316 mmol) was first dissolved in 1 mL of toluene. In another round bottom flask, PbO (0.3 g, 1.3 mmol) and oleic acid (1.5 mL, 4.7 mmol) was dissolved in 18 mL of octadecene and degassed at 100 °C under vacuum overnight to form Pb-oleate. In a separate flask, bis(trimethylsilyl) sulfide (TMS) (0.29 mL, 1.37 mmol) was dissolved in 13 mL of degassed octadecene. The Pb-oleate solution was heated to 63 °C, and then the TMS solution was injected rapidly to enable nucleation of the PbS-QDs. After the initial synthesis of the oleic acid capped PbS QDs, the FMT solution was injected into the flask at 60 °C during the cooling stage of the reaction. The reaction was further cooled to 30 °C, and acetone was injected into the flask to precipitate the QDs. The FMT-QDs were centrifuged at 7800 rpm for 5 minutes, and the precipitate was redispersed in toluene. These FMT-QDs were precipitated again with acetone, and dried under vacuum for 20 minutes. The FMT-QDs were then dissolved in anhydrous octane at 50 mg mL^{-1}.

Full device preparation

Two layers of ZnO nanoparticles were spin coated onto an ITO substrate at 3000 rpm for 30 s. The synthesis of these ZnO nanoparticles is discussed elsewhere.[7] Then a 315 mg mL^{-1} of a $PbI_{0.8}Br_{0.2}$-PbS active layer was spin coated onto the top of the ZnO nanoparticles. The synthesis and ligand exchange method for these $PbI_{0.8}Br_{0.2}$-PbS QDs is discussed elsewhere.[16] Then two layers of EDT-PbS were spin coated onto the active layer. The methods are discussed below:

Direct soak EDT-PbS QDs

The preparation of the EDT-PbS QD exchange was performed as described in a previous study.[16] To prepare one layer of EDT-PbS QDs, a 50 mg mL^{-1} solution OA-QDs were spin coated at 2500 rpm for 10 s onto the top of a PbS-active layer. The OA-QD layer was then soaked in a 0.01% v/v solution of 1,2-ethanedithiol (EDT) in acetonitrile for 30 s. The solution was then spin coated off at 2500 rpm, and washed three times with acetonitrile. These steps were repeated twice to yield 2 layers of EDT-PbS.

FMT-cleaved EDT-PbS QDs

The FMT-QDs initially dispersed in toluene were precipitated with the addition of acetone. The QDs were further dried and dispersed in octane at a concentration of 50 mg mL^{-1} The FMT-QDs were spin coated on top of a PbS-active layer at a spin speed of 2500 rpm for 10 s. The FMT-QD layer is then treated with mild base solution noted below in ethyl acetate for 30 s. The device was then spun at 2500 rpm for 10 s to

remove the residual solvent. The film was washed 3 additional times with ethyl acetate.

FMT mild base preparation

Mixtures of bases were prepared at a 1% v/v solution in ethyl acetate. For example, a 9 : 3 mixture of DTP : DBU is as follows: 100 μL of DTP is diluted in 10 mL of ethyl acetate. In a separate vial, 100 μL of DBU is dissolved in 10 mL of ethyl acetate. Then 900 μL of the 1% DTP solution is mixed with 300 μL of the 1% DBU solution yield a 9 : 3 DTP : DBU mixture.

For the 30 : 1 DMPpy : DBU mixture, 100 μL of DMPpy is diluted in 10 mL of ethyl acetate. In a separate vial, 100 μL of DBU is dissolved in 10 mL of ethyl acetate. Then 900 μL of the 1% DMPpy solution is mixed with 30 μL of the 1% DBU solution to yield a 30 : 1 DMPpy : DBU mixture.

Absorbance characterization

Film Absorbance measurements were performed by a Lambda 950 500 UV-Vis-IR spectrometer.

Fourier transform infrared (FTIR) spectroscopy measurements

Attenuated total reflectance (ATR) FTIR measurements were performed on a Thermo Nicolet is 50.

UPS measurements

A thin layer of colloidal QDs was spin-coated at 2500 rpm onto an Au substrate before UPS testing. The ultraviolet photo-electron spectra were obtained using the 21.22 eV He I lines from the discharge lamp. The band gaps for both the EDT-PbS film and cFMT-PbS film were determined by the optical absorption spectrum by taking the value from their first excitonic peaks. The Fermi level for each film were taken from the intersection from the slope of the low binding energy section and its baseline, and subtracted from the He I line. The value of the valence band maximum was determined by adding the Fermi level and the value from the intersection from the slope of the high binding energy section and its baseline. The value of the conduction band minimum was determined by adding the value of the valence band maximum and the optical band gap.

XPS characterization

A layer of colloidal QDs were spin-coated at 2500 rpm onto a glass substrate before XPS measurements. The film was then mounted onto a stainless steel mounting plate. XPS measurements were performed on a Thermo Scientific K-Alpha system. The source used was an Al Kα source. The takeoff angle was 90°. In order to account for charging, XPS spectra were calibrated to the samples' respective C 1s peak at 284.8 eV.

AM1.5 measurements

AM1.5 current voltage (*J*–*V*) sweeps were collected using a Keithley 2400 sourcemeter unit under simulated AM1.5G illumination (Sciencetech class A). The AM1.5 was calibrated using a reference solar cell (Newport). The devices were measured under a continuous flow of nitrogen gas. The aperture was 4.9 mm^2 for a device.

External quantum efficiency (EQE) measurements

EQE measurements are performed with an Oriel Instruments Quantum Efficiency measurement system.

Scanning electron microscope (SEM) imaging measurements

SEM images were taken using the Hitachi SU5000 microscope with an accelerating voltage of 5 kV.

DFT calculations

All DFT calculations were performed using Gaussian 09. B3LYP was used as the functional and all molecules were optimized to a basis set of 6-311g**.

Results and discussion

In designing a ligand tailored for the application of an uniform film, we pursued the Fmoc protecting group since it (1) can be combined with the commonly used EDT, (2) provides colloidal stability for the QDs after homogenous ligand exchange, (3) can be cleaved with a mild base that does not interfere with the QD surfaces, (4) can be synthesized on the gram scale in a one-step synthesis, (5) is a short ligand which facilitates dense QD packing, and (6) it forms, upon deprotection of the ligand, byproducts that are electronically and chemically inert to the QD surfaces, in particular avoiding carboxylic acids which have been shown to be problematic in PbS photovoltaics.[21] Fmoc deprotection has been studied previously in a many reports for various applications.[32–35] The FMT deprotection mechanism for this reaction is detailed in Fig. 1. The most acidic proton residing on the cyclopentyl ring within the Fmoc protecting group is first deprotonated by a mild base (1,8-diazabicyclo(5.4.0)undec-7-ene, DBU). This causes the electrons to break the dibenzofulvene bond by forming the unstable carbonothioate in solution, which quickly decomposes into CO_2 and EDThiolate. The dibenzofulvene byproduct, a highly reactive byproduct, then reacts with a nearby nucleophile (2,6-dimethylpiperidine, DMPpy) to form an inert molecule. In this report DBU was used in catalytic amounts to perform the initial deprotonation of the Fmoc group, while DMPpy was used as a sterically hindered nucleophile for reaction with the dibenzofulvene adduct.[27]

The synthesis of OA-PbS followed the procedure reported by Hines and Scholes[31] and was slightly modified for this study (see Experimental). After synthesis and film deposition, Fmoc cleavage or EDT ligand exchange was performed on the respective films, and we used surface analysis techniques to verify that the reaction did indeed go to completion. Similar absorbance values for both FMT-PbS and OA-PbS films suggest that both films have similar thicknesses. The FMT-PbS film is comparatively red-shifted as has been observed for other systems upon ligand exchange with EDT.[36] The absorbance of both films increased after their conversion to cFMT-PbS or EDT-PbS QD films (Fig. 2a). Previous studies have suggested that the optical density of PbS films increases after ligand exchange reactions when the exchanged QDs are more densely

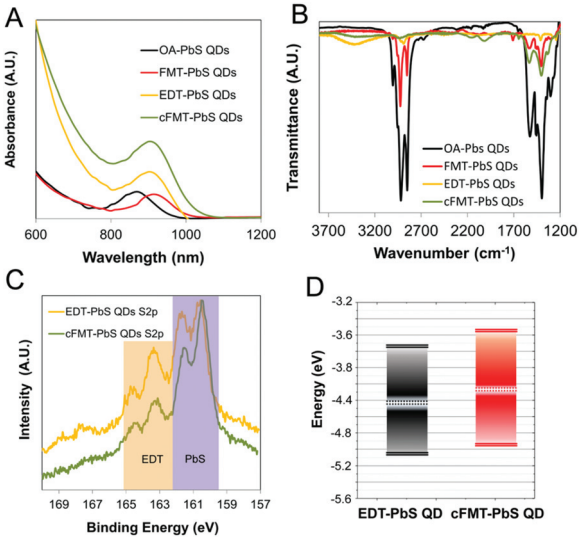

Fig. 2 (A) Absorbance spectra of QD films: OA-PbS (black), FMT-PbS (red), EDT-PbS films made by the conventional method (yellow), and cFMT-PbS films (green). (B) FTIR spectra QD films: OA-PbS (black, scaled to one third intensity for comparison), FMT-PbS (red), EDT-PbS films made by the conventional method (yellow), and cFMT-PbS films (green). (C) XPS sulfur 2p spectra comparing the EDT-PbS film (yellow) and cFMT-PbS film (green) (D) band structure determined by UPS and absorbance results comparing the band alignments of an EDT-PbS film (black) and a cFMT-PbS film (red).

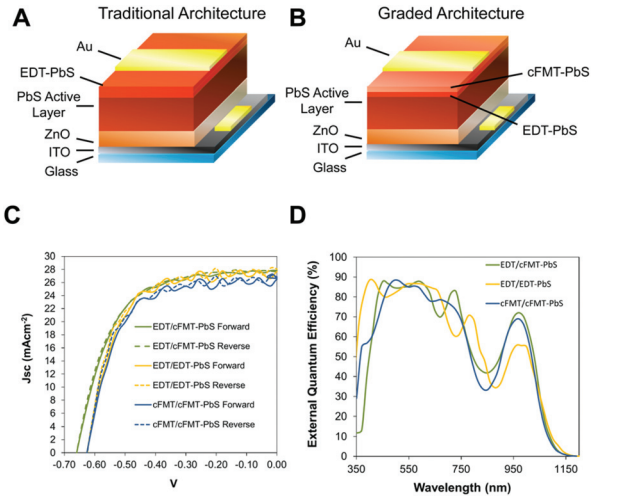

Fig. 3 (A) Solar cell architecture using only the conventional EDT exchange method. (B) Solar cell architecture utilizing both the traditional EDT exchange method and the FMT exchange method. (C) *J*–*V* curves for FMT-colloidal QDs (black) and traditional OA-colloidal QDs (grey). (D) External quantum efficiency measurements comparing the devices fabricated with an FMT-colloidal QD and traditional OA-colloidal QDs.

packed.[37] When comparing the two absorption spectra in Fig. 2a, the optical density increased more for cFMT-PbS QD films than for EDT-PbS QD films implying a higher packing density of the QDs. The increased absorbance at the exciton peak is also reflected later in the External Quantum Efficiency measurements of the prepared devices (*vide infra*) (Fig. 3d).

Fourier transform infrared (FTIR) spectroscopy reveals a decrease in organic content after each QD functionalization. In particular, the C–H stretches (2850–3000 cm^{-1}) were reduced successively between OA-PbS, FMT-PbS and cFMT-PbS. A broad –OH peak appears at 3500 cm^{-1} for the EDT-PbS QD film which can be attributed to the fabrication process of EDT-PbS; the direct soak EDT solvent, acetonitrile, is hydroscopic which allows for atmospheric moisture to be absorbed into the film.[38]

X-ray photoelectron spectroscopy (XPS) measurements were used to determine the surface composition of the EDT-PbS and cFMT-PbS QD films (Fig. S5†). The spin orbit coupled sulfur 2p3/2 and sulfur 2p1/2 peaks appearing at around 160.4 eV and 161.7 eV shown in Fig. 2c match closely to that of PbS.[10] The pair of peaks at 163.5 and 164.7 eV corresponds to thiolates of EDT bound to the PbS surface. It is worth noticing that when intensities are normalized to PbS S2p peaks, the peaks originating from EDT S2p peaks are of much greater intensity for the EDT-PbS compared to the cFMT-PbS suggesting more ligand present in the EDT-PbS film, which further suggests that the increased absorbance for the cFMT-PbS is implied from increased QD packing. The peaks in the Pb 4f and C 1s spectra of both films match closely (Fig. S5†). In the O 1s spectra, both films show the expected lead oxide species due to air exposure at 530.7 eV,[39] but an additional peak at 532.6 eV was only observed for the EDT-PbS films, which is attributed to lead oleate species (Fig. S5†).[40,41] The presence of carboxylate suggests an incomplete EDT ligand exchange and/or oleate removal during the fabrication of the direct soak EDT film. The lack of a carboxylate signal on the cFMT-PbS O 1s spectra suggests that the homogeneous ligand exchange successfully displaced all of the oleic acid.

The electronic properties of cFMT-PbS QD films and their EDT-PbS counterparts were analyzed using ultraviolet photoelectron spectroscopy (UPS) (Fig. 2d and S6†). The determination of the valence band maximum, conduction band minimum, and Fermi level for each films are discussed in detail in the Experimental section. The bandgaps for the EDT-PbS QD film and the cFMT-PbS QD film were 1.35 eV (λ_{ex} = 918.5 nm) and 1.41 eV (λ_{ex} = 880 nm), respectively. The position of the bandgap for the EDT-PbS QD film matches well with those reported in literature, while the cFMT-PbS film measurements showed a shallower band position than EDT-PbS.[14,15] For these similar sized CQDs, the in-synthesis FMT exchange for oleic acid results in a more complete thiolate packing on the QD surface, producing a shallower band position. The shallower position of the conduction band as seen in the cFMT-PbS QD film may allow for further electron blocking when used as a hole transport layer in a typical inverted QD solar cell. A good electron blocking layer will decrease the chance of charge recombination at the Au contact, and successfully transport holes to the anode.[14,16,42]

We used the cFMT-PbS QDs as a HTL for PbS solar cells. A conventional PbS solar cell architecture is indium doped tin

oxide (ITO)/zinc oxide (ZnO)/PbS-Active layer/EDT-PbS/Au (Fig. 3a).[7,14,16] The specific method for producing the ZnO electron transport layer and PbS active layer has been discussed in previous literature.[16] In the conventional QD PV device, two layers of solid-state exchanged EDT-PbS (50 nm in total) were applied onto the top of the active layer to serve as the HTL.[14] Herein, we replaced the traditional HTL with our cFMT-PbS layers while keeping the rest of the device architecture unchanged.

To enable a working HTL, the Fmoc protecting group was cleaved using a mixture of DBU and a second weaker base. In this reaction, DBU is used as a catalytic base, while the second molecule acts as an electrophilic agent to remove the dibenzofulvene byproduct.[27] The solar cell figures of merit, open circuit voltage (V_{oc}), short circuit current density (J_{sc}), fill factor (FF), and power conversion efficiencies (PCEs) are listed in Table S5† for three base treatment protocols. A large variation in PCEs was observed when the second weaker base was changed, and the performance of these devices was compared to the control device. The best control device utilizes EDT/EDT-PbS QDs for the HTL and had a PCE of 11.01%. When FMT-PbS HTLs were soaked with only a 1% v/v DBU solution and no secondary base, a device with a PCE of 7.8% was produced. We hypothesize the reduction in performance is due to residual DBU, dibenzofulvene, or uncleaved Fmoc left within the film even after the washing procedure. The combination of lower V_{oc}, J_{sc}, and FF indicate that the device has poor charge extraction at the HTL surface. Per Fig. 1, DBU is responsible for performing the initial deprotonation leading to cleavage of the Fmoc group. However, as a non-nucleophilic base, it will not readily react with dibenzofulvene, and steps of the cleavage may reverse and therefore produce an incomplete cleavage.[43] While the addition of a nucleophile to the treatment protocol is needed, careful consideration must be given to the molecular electronics and sterics. When the base/nucleophile combination of a 1% solution of 9 : 2 v/v 2,6-lutidine and DBU were used to remove the dibenzofulvene byproduct, a device was produced with a PCE of only 5.8%. Unfortunately, the electron rich nitrogen group of 2,6-lutidine likely performs a ligand exchange with the QD surfaces, similar to those seen previously with butylamine.[44–46] The 2,6-lutidine as a surface ligand may diminish charge transport between QDs, lowering the overall performance of the device. Due to this issue, we hypothesized that a similar molecule with a bulkier side chain may actually avoid ligand exchange on the surface of the QDs due to steric hindrance but still be able to react with the dibenzofulvene. Therefore, the choice of 2,6-ditertbutylpyridine (DTP) was a good replacement over the smaller 2,6-lutidene. For this specific device, the optimized concentration of 1% 9 : 3 v/v DTP : DBU was employed. This device exhibited a noticeably higher J_{sc} over the other FMT-based devices (27 mA cm^{-2} *vs.* 20 mA cm^{-2}), and an overall PCE of 9.56%. External quantum efficiency (EQE) measurements reveal that improvement of the J_{sc} for the cFMT-PbS QD devices are enhanced mainly in the height of the exciton peak (Fig. 3d). However, a slightly lower V_{oc} for this cFMT-PbS device hints that the cFMT-PbS/PbS active layer may have more interface traps from trace organic residue from the cFMT-PbS treatment. Further optimization of the deprotection procedure may mitigate this problem in future.

From UPS studies as seen in Fig. 2d, we observed that band positions of the cFMT-PbS QD films are shallower than the EDT-PbS counterparts. Therefore, we employed a graded HTL architecture designed as EDT/cFMT-PbS as seen in Fig. 3b. Graded HTLs architectures can create an energy landscape that facilitates hole transport and has been used previously to improve the efficiency of PbS-QD solar cells by effectively extending the depletion width in the main absorber layer.[14,47] In this scenario, one traditional EDT-PbS layer is fabricated followed by the addition of an FMT-PbS layer which is then cleaved with base (DBU) and nucleophile (2,6-dimethylpiperidine, DMPpy), a molecule chosen for its improved ability to react with dibenzolfulvene due to its lack of aromaticity. Cross sectional scanning electron microscope (SEM) images reveal that the both the EDT/EDT and EDT/cFMT devices yield similar thicknesses in both the active layer and HTL (Fig. S10†). The SEM images shown in Fig. S10† of the EDT-PbS and cFMT-PbS devices suggest that the CQDs are too densely packed in both devices to be resolved by the SEM imaging. PbS QDs used for both the EDT-PbS and cFMT-PbS cases are passivated by the same short ligands, 1,2-ethanedithiol. Therefore, the more intense absorbance spectra and the increased XPS intensity of sulphur 2p3/2 and 2p1/2 peaks of the cFMT-PbS CQDs over the EDT-PbS implies that the packing is improved (Fig. 2a and c). The best device produced in this fashion yielded a performance of 11.0%, comparable to EDT/EDT-PbS control devices which also showed PCEs of 11.0%. This device had an improved V_{oc} from a cFMT/cFMT-PbS QD device because the mild FMT cleavage treatment does not disrupt the EDT-PbS CQDs. It is important to deposit the HTL to the PbS-CQD active layer in ambient conditions instead of an inert atmosphere, as mild oxygen doping for HTLs is known for improving device performance (inert atmosphere fabricated devices shown in Fig. S8, Table S2†).[48]

The series resistance for dark *J–V* sweeps was compared for the aged EDT/cFMT and EDT/EDT devices. The EDT/cFMT devices showed a lower series resistance (2.9 Ω cm^2 compared to 6.4 Ω cm^2 for EDT/EDT devices), which is indicative of improved hole transport (Fig. S11†).[49] The external quantum efficiency (EQE) plots reveal enhancements at the exciton peak for both the EDT/cFMT-PbS and EDT/EDT-PbS QD devices (Fig. 3d). The stability of EDT/cFMT devices is better than the EDT/EDT device. The PCE of the EDT/cFMT device stored in air over a period of 18 days (approximately 430 hours) lost 1.8 absolute power points in PCE, whereas the EDT/EDT device lost 2.2 absolute power points in PCE (Table S3, S4 and S6†). The evolution of PCE over the 18 day storage period was plotted (Fig. S12†). The EDT/cFMT device maintained its PCE after six days of air storage, while the EDT/EDT device started to decrease by 0.4%. We attribute this improvement to improved thiol passivation on the PbS surface when using the FMT protocol; by performing a homogenous ligand exchange

in solution, greater ligand coverage is achieved.[19–21,23,50] This method still benefits from the uniform film provided by the traditional native-ligand stabilized PbS QD film deposition.

Conclusions

In conclusion, an alternative method to produce EDT-functionalized PbS QD films was devised through an alternative protection and deprotection step of EDT. The native OA ligands of PbS were completely exchanged in solution by a FMT ligand to yield colloidal FMT-capped QDs. These FMT-QDs were used to construct a hole transport layer in PVs. The Fmoc protecting group of the FMT ligand was easily removed by a mild base treatment, and a pristine EDT-PbS film was produced. Films with denser QD packing, fewer carboxylate-impurities, greater thiol ligand coverage, and shallower band position were produced through the FMT cleavage method than the traditional EDT ligand exchange method. By developing a graded device architecture using first the traditional EDT-PbS and then a cFMT-PbS QD film, a QD device with comparable performance to controls but improved longevity was produced. This work provides important insight into the necessity of improving the HTL and highlights the role that chemistry on the surface of QDs affects their electronic properties.

Conflicts of interest

The authors state that there are no conflicts to declare.

Acknowledgements

The authors thank D. Kopilovic, E. Palmiano, and R. Wolowiec for their assistance over the course of this research. This research was funded by the United States of America National Science Foundation (NSF EPS-1004083), Natural Sciences and Engineering Research Council of Canada (NSERC), Alexander Graham Bell Canada Graduate Scholarships-Doctoral Program (CGS-D), Materials for Enhanced Energy Technologies (MEET) scholarships, the Mitchum Warren Fellowship and the Beckman Scholars Program.

Notes and references

1 G. H. Carey, A. L. Abdelhady, Z. Ning, S. M. Thon, O. M. Bakr and E. H. Sargent, *Chem. Rev.*, 2015, **115**, 12732–12763.
2 F. P. García de Arquer, A. Armin, P. Meredith and E. H. Sargent, *Nat. Rev. Mater.*, 2017, **2**, 16100.
3 F. Fan, O. Voznyy, R. P. Sabatini, K. T. Bicanic, M. M. Adachi, J. R. McBride, K. R. Reid, Y.-S. Park, X. Li, A. Jain, R. Quintero-Bermudez, M. Saravanapavanantham, M. Liu, M. Korkusinski, P. Hawrylak, V. I. Klimov, S. J. Rosenthal, S. Hoogland and E. H. Sargent, *Nature*, 2017, **544**, 75–79.
4 X. Dai, Z. Zhang, Y. Jin, Y. Niu, H. Cao, X. Liang, L. Chen, J. Wang and X. Peng, *Nature*, 2014, 96–99.
5 R. Wang, Y. Shang, P. Kanjanaboos, W. Zhou, Z. Ning and E. H. Sargent, *Energy Environ. Sci.*, 2016, **9**, 1130.
6 A. H. Ip, S. M. Thon, S. Hoogland, O. Voznyy, D. Zhitomirsky, R. Debnath, L. Levina, L. R. Rollny, G. H. Carey, A. Fischer, K. W. Kemp, I. J. Kramer, Z. Ning, A. J. Labelle, K. W. Chou, A. Amassian and E. H. Sargent, *Nat. Nanotechnol.*, 2012, **7**, 577–582.
7 X. Lan, O. Voznyy, F. P. García De Arquer, M. Liu, J. Xu, A. H. Proppe, G. Walters, F. Fan, H. Tan, M. Liu, Z. Yang, S. Hoogland and E. H. Sargent, *Nano Lett.*, 2016, **16**, 4630–4634.
8 N. Zhang, D. C. J. Neo, Y. Tazawa, X. Li, H. E. Assender, R. G. Compton and A. A. R. Watt, *ACS Appl. Mater. Interfaces*, 2016, **8**, 21417–21422.
9 X. Zhang, J. Zhang, D. Phuyal, J. Du, L. Tian, V. A. Öberg, M. B. Johansson, U. B. Cappel, O. Karis, J. Liu, H. Rensmo, G. Boschloo and E. M. J. Johansson, *Adv. Energy Mater.*, 2016, 1702049.
10 Y. Cao, A. Stavrinadis, T. Lasanta, D. So and G. Konstantatos, *Nat. Energy*, 2016, **1**, 16035.
11 Y. Bi, S. Pradhan, S. Gupta, M. Z. Akgul, A. Stavrinadis and G. Konstantatos, *Adv. Mater.*, 2018, **30**, 1–6.
12 J. Gao, C. L. Perkins, J. M. Luther, M. C. Hanna, H. Y. Chen, O. E. Semonin, A. J. Nozik, R. J. Ellingson and M. C. Beard, *Nano Lett.*, 2011, **11**, 3263–3266.
13 G. H. Carey, L. Levina, R. Comin, O. Voznyy and E. H. Sargent, *Adv. Mater.*, 2015, **27**, 3325–3330.
14 C.-H. M. Chuang, P. R. Brown, V. Bulović and M. G. Bawendi, *Nat. Mater.*, 2014, **13**, 1–6.
15 P. R. Brown, D. Kim, R. R. Lunt, N. Zhao, M. G. Bawendi, J. C. Grossman and V. Bulović, *ACS Nano*, 2014, **8**, 5863–5872.
16 M. Liu, O. Voznyy, R. Sabatini, F. P. García De Arquer, R. Munir, A. H. Balawi, X. Lan, F. Fan, G. Walters, A. R. Kirmani, S. Hoogland, F. Laquai, A. Amassian and E. H. Sargent, *Nat. Mater.*, 2017, **16**, 258–263.
17 J. Kim, O. Ouellette, O. Voznyy, M. Wei, J. Choi, M. Choi, J. W. Jo, S. Baek, J. Fan and M. I. Saidaminov, *Adv. Mater.*, 2018, **30**, 1803830.
18 J. Xu, O. Voznyy, M. Liu, A. R. Kirmani, G. Walters, R. Munir, M. Abdelsamie, A. H. Proppe, A. Sarkar and F. P. G. de Arquer, *Nat. Nanotechnol.*, 2018, 1.
19 D. Zherebetskyy, M. Scheele, Y. Zhang, N. Bronstein, C. Thompson, D. Britt, M. Salmeron, P. Alivisatos and L. W. Wang, *Science*, 2014, **344**, 1380–1384.
20 M. A. Boles, D. Ling, T. Hyeon and D. V. Talapin, *Nat. Mater.*, 2016, **15**, 141–153.
21 G. H. Carey, I. J. Kramer, P. Kanjanaboos, G. Moreno-Bautista, O. Voznyy, L. Rollny, J. A. Tang, S. Hoogland and E. H. Sargent, *ACS Nano*, 2014, **8**, 11763–11769.

22 J. M. Luther, M. Law, Q. Song, C. L. Perkins, M. C. Beard and A. J. Nozik, *ACS Nano*, 2008, **2**, 271–280.
23 G. A. Bagiyan, I. K. Koroleva, N. V. Soroka and A. V. Ufimtsev, *Russ. Chem. Bull.*, 2003, **52**, 1135–1141.
24 A. H. Ip, A. J. Labelle and E. H. Sargent, *Appl. Phys. Lett.*, 2013, **103**, 1–4.
25 G. H. Carey, M. Yuan, R. Comin, O. Voznyy and E. H. Sargent, *ACS Appl. Mater. Interfaces*, 2015, 21995–22000.
26 M. J. Turo and J. E. Macdonald, *ACS Nano*, 2014, **8**, 10205–10213.
27 K. Ralhan, V. G. KrishnaKumar and S. Gupta, *RSC Adv.*, 2015, **5**, 104417–104425.
28 A. K. Tickler, C. J. Barrow and J. D. Wade, *J. Pept. Sci.*, 2001, **7**, 488–494.
29 R. Behrendt, P. White and J. Offer, *J. Pept. Sci.*, 2016, **22**, 4–27.
30 X. Yong and M. A. A. Schoonen, *Am. Mineral.*, 2000, **85**, 543–556.
31 M. A. Hines and G. D. Scholes, *Adv. Mater.*, 2003, **15**, 1844–1849.
32 L. A. Carpino and G. Y. Han, *J. Org. Chem.*, 1972, **37**, 3404–3409.
33 M. Amblard, J.-A. Fehrentz, J. Martinez and G. Subra, *Mol. Biotechnol.*, 2006, **33**, 239–254.
34 J. S. Lindsey, S. Prathapan, E. Johnson, R. W. Thomas and R. W. Wagner, *Tetrahedron*, 1994, **50**, 8941–8968.
35 M. Schnoelzer, P. Alewood, A. Jones, D. Alewood and S. B. Kent, *Int. J. Pept. Protein Res.*, 1992, **40**, 180–193.
36 E. M. Miller, D. M. Kroupa, J. Zhang, P. Schulz, A. R. Marshall, A. Kahn, S. Lany, J. M. Luther, M. C. Beard, C. L. Perkins and J. Van De Lagemaat, *ACS Nano*, 2016, **10**, 3302–3311.
37 A. H. Ip, A. Kiani, I. J. Kramer, O. Voznyy, H. F. Movahed, L. Levina, M. M. Adachi, S. Hoogland and E. H. Sargent, *ACS Nano*, 2015, **9**, 8833–8842.
38 J. Tang, X. Wang, L. Brzozowski, D. A. R. Barkhouse, R. Debnath, L. Levina and E. H. Sargent, *Adv. Mater.*, 2010, **22**, 1398–1402.
39 V. B. Crist, *Handbook of Monochromatic XPS Spectra*, John Wiley & Sons, Ltd., West Sussex, England, 2000.
40 S. Biniak, G. Szymański, J. Siedlewski and A. Świątkowski, *Carbon*, 1997, **35**, 1799–1810.
41 Q. Feng, W. Zhao, S. Wen and Q. Cao, *Sep. Purif. Technol.*, 2017, **178**, 193–199.
42 Z. Yang, A. Janmohamed, X. Lan, F. P. García De Arquer, O. Voznyy, E. Yassitepe, G. H. Kim, Z. Ning, X. Gong, R. Comin and E. H. Sargent, *Nano Lett.*, 2015, **15**, 7539–7543.
43 J. E. Sheppeck, H. Kar and H. Hong, *Tetrahedron Lett.*, 2000, **41**, 5329–5333.
44 J. S. Owen, J. Park, P. E. Trudeau and A. P. Alivisatos, *J. Am. Chem. Soc.*, 2008, **130**, 12279–12281.
45 A. J. Morris-Cohen, M. D. Donakowski, K. E. Knowles and E. A. Weiss, *J. Phys. Chem. C*, 2010, **114**, 897–906.
46 M. L. Böhm, R. J. P. Kist, F. S. F. Morgenstern, B. Ehrler, S. Zarra, A. Kumar, Y. Vaynzof and N. C. Greenham, *Adv. Energy Mater.*, 2014, **4**, 1400139.
47 N. Zhijun, Z. David, A. Valerio, S. Brandon, X. Jixian, V. Oleksandr, M. Pouya, L. Xinzheng, H. Sjoerd, R. Yuan and S. E. H. Sargent, *Adv. Mater.*, 2013, **25**, 1719–1723.
48 A. R. Kirmani, A. D. Sheikh, M. R. Niazi, M. A. Haque, M. Liu, F. P. G. de Arquer, J. Xu, B. Sun, O. Voznyy, N. Gasparini, D. Baran, T. Wu, E. H. Sargent and A. Amassian, *Adv. Mater.*, 2018, **30**, 1–9.
49 S. W. Baek, S. H. Lee, J. H. Song, C. Kim, Y. S. Ha, H. Shin, H. Kim, S. Jeong and J. Y. Lee, *Energy Environ. Sci.*, 2018, **11**, 2078–2084.
50 J. M. Luther, M. Law, Q. Song, C. L. Perkins, M. C. Beard and A. J. Nozik, *ACS Nano*, 2008, **2**, 271–280.